Cannabinoid-inspired Inhibitors of Autotaxin

Mathias Christophe Eymery, Kim-Anh Nguyen, Shibom Basu, Jens Hausmann, Viet-Khoa Tran Nguyen, Hans Peter Seidel, Lola Gutierrez, Ahcène Boumendjel,* and Andrew Aloysius McCarthy*

ABSTRACT: Autotaxin (ATX) is an enzyme primarily known for the production of lysophosphatidic acid. Being involved in the development of major human diseases, such as cancer and neurodegenerative diseases, the enzyme has been featured in multiple studies as a pharmacological target. We previously found that the cannabinoid tetrahydrocannabinol (THC) could bind and act as an excellent inhibitor of ATX. This study aims to use the cannabinoid scaffold as a starting point to find cannabinoid-unrelated ATX inhibitors, following a funnel down approach in which large chemical libraries sharing chemical similarities with THC were screened to identify lead scaffold types for optimization. This approach allowed us to identify compounds bearing chromone and indole scaffolds as promising ATX inhibitors. Further optimization led to MEY-003, which is characterized by the direct linkage of an *N*-pentyl indole to the 5,7-dihydroxychromone moiety. This molecule has potent inhibitory activity towards ATX-β and ATX-ɣ as evidenced by enzymatic studies and its mode of action was rationalized by structural biology studies.

Graphical Abstract

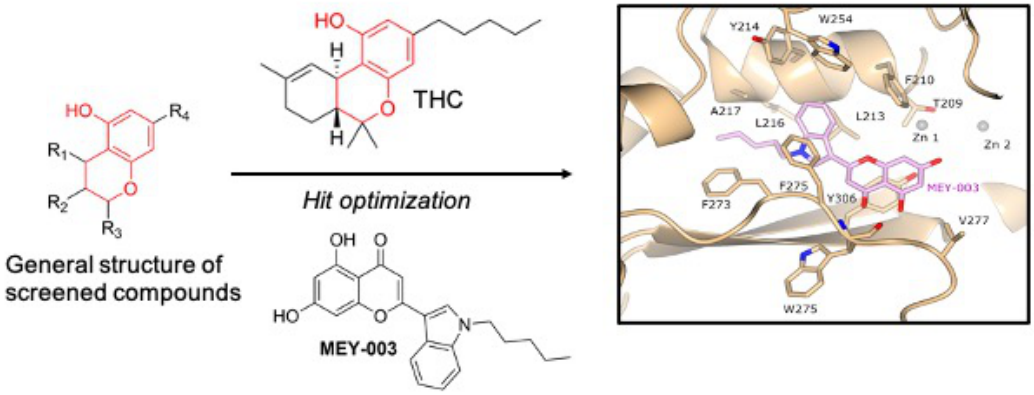

■ INTRODUCTION

Autotaxin (ATX) is a 115-125 kDa lysophospholipase D involved in a large range of physiological and pathological processes.[1] This enzyme is part of the ectonucleotide pyrophosphatase/phosphodiesterase family and is also referred to as ENPP2. ATX is mainly involved in the phospholipidic metabolism and the production of extracellular lysophosphatidic acid (LPA) from lysophophatidylcholine (LPC).[2] At least five human isoforms have been discovered so far.[3] The β isoform is the most abundant, expressed in many parts of the body and accounting for the majority of ATX activity. The α and ε isoforms are less abundant and differ from ATX-β by a 52 amino acid (aa) polybasic insertion.[4] The ATX delta isoform is missing an exon of 19 tetrapeptides with unknown function.[5] ATX-ɣ is brain-specific and differs from ATX-β by a 25 aa insertion, while its activity is similar to the β isoform (Figure 1).[3] The ATX structure has been widely studied with 51 experimental entries in the Protein Data Bank to date.[6] It relies on (i) two flexible somatomedin B (SMB)-like domains, involved in protein-protein interactions, (ii) a conserved phosphodiesterase domain responsible for catalytic activity, and (iii) an inactive nuclease domain (Figure 1).[7] Structural insights into ATX show that the active site contains two zinc ions, allowing lysophosphatidylcholine binding and cleavage. A major point of substrate recognition by the ATX active site is the presence of a hydrophobic pocket, allowing the accommodation of both LPA and LPC.[7]

The implication of ATX in a large range of human diseases can be highlighted by both fundamental research and clinical trials.[2,3,8–10] Firstly, it has been shown that ATX is important for cancer progression and metastasis as this enzyme is responsible for LPA generation.[8,9,11] LPA is a growth factor, regulating many different cellular functions, some of which are important for malignant cells. Notably, it has been shown that LPA is a cell motility factor and that inhibiting ATX results in a decrease of *in vitro* cellular invasion through a decrease of LPA concentration in the surrounding fluids.[10] *In vivo* experiments and clinical trials showed that ovarian cancer cells produce high levels of LPA, as well as other conditions like during pregnancy,[12] stroke[13], bone diseases[14] and acute coronary syndrome.[15] Recently, the confirmation of ATX's implication in neurological diseases was reported.[11,16] Further studies showed that ATX

levels are related to metabolism disorders in Alzheimer's disease, highlighting ATX as an interesting biomarker for this devastating pathology.[17] ATX levels in the serum were compared to MRI data of patients suffering from this disease, showing that some features of the latter were correlated with the former.[17] Serum levels of ATX also vary in other diseases and physiological conditions, which strengthens the need for fine-tuning of ATX catalysis.[8] However, while systemic LPA generation by ATX can be used as a biomarker it is not freely available in the blood, and unable to cross physiological compartments. In addition, LPA levels are not necessarily elevated in patients with cancer as the secretion and binding is mostly limited to tumor sites.[3] Also, LPA binds to receptors expressed at the cell surface. These receptors have many functions, e.g. regulating cell survival, apoptosis, cell differentiation, malignant transformation and many other processes through their G protein-coupled receptor activity.[18] More precisely, LPA receptors from the EDG family (LPA1 to LPA3) have been widely studied and are major pharmacological targets. Non-EDG family LPA receptors (LPA4-LPA6) were reported and recent studies allowed LPA6 structure determination and described this receptor family as important drug targets[19]. In recent years, it has been hypothesized and demonstrated that ATX may act not only as an enzyme but also as a chaperone presenting LPA to its receptors.[7,20] In this setting, it is of great interest to develop drugs that could selectively inhibit ATX in its pathological environment, without decreasing the overall levels of LPA in the blood.

Various ATX inhibitors have already been developed and some are now in clinical trials.[2,21–23] However, compounds with satisfactory pharmacokinetics parameters and low toxicity are limited. There is still no approved drug for ATX brain-related diseases. Moreover, ATX distribution is tissue-specific and most of the research has been focused on the α and β isoforms. For ATX-γ, plausibly related to many neurological diseases, a deeper understanding is needed to design and develop more specific inhibitors of this isoform and to fully understand its pathophysiological role.

Recently, we discovered that ATX was inhibited by various cannabinoids. In particular, THC and delta 6a,10a-THC inhibited ATX as mixed-type inhibitors at nanomolar concentrations.[24] Pharmacokinetic parameters for cannabinoids are widely studied and there is a consensus that they cross the blood brain

barrier and bind to CB1 and CB2 receptors, making them an ideal starting point to specifically inhibit ATX in the brain. Although cannabinoids were revealed as excellent ATX inhibitors, their major drawbacks relate to regulations, legislation and acceptance by patients, making them less desirable for development.

In this study, we used the results obtained with cannabinoids for the identification and development of new inhibitors devoid of potential side effects. Here, we identified a new family of potent ATX inhibitors through the screening of chemical libraries sharing structural similarities with THC. We also report the human ATX-ɣ structure bound to the most active inhibitor (namely here MEY-003), a novel ATX inhibitor bearing both chromone and indole scaffolds, and LPA at atomic resolutions using X-ray crystallography.

Figure 1. Schematic comparison of the ATX-β and ATX-ɣ isoforms.

■ RESULTS

Identification of hits by the screening of compounds sharing structural similarities with cannabinoid. Our strategy was based on the structural similarity between the benzopyran moiety of THC and THC-unrelated molecules bearing this chemical entity. Among these compounds, we targeted chromone-bearing derivatives (Figure 2). This druggable scaffold is known for its therapeutic potential and safety. The therapeutic potential of chromone was recently highlighted in two major reports.[25,26] Herewith, 80 compounds bearing a chromone and chromone-like moieties were tested for their inhibitory potential at 1 μM. The most important representatives of the screened compounds are available in supplementary information section II. The screening revealed that molecules bearing an indole linked to a chromone

moiety presented the highest inhibition against ATX (Figure 2). Following further structure-activity relationship (SAR) studies and optimization, we found that compounds having the following substitution pattern tended to exert a high inhibitory effect: (a) the presence of a linear hydrophobic substituent at the indole nitrogen, (b) the presence of two hydroxyls at positions 5/7 of the chromone moiety (Figure 2), (c) the addition of a hydroxyl group at position 3 of chromone was harmful for the inhibition activity (Table S1), (d) the site of linkage of chromone and indole moieties is crucial since when the linkage was done through the phenyl ring of the indole moiety (MEY-005), the inhibition activity was decreased (Table 1), (e) the benzopyranone moiety of chromone is important as its shift to a benzofuran led to drop of activity. Interestingly, the length of hydrophobic carbon chain inducing the highest inhibition activity correlates with the one found in THC. Branched chains, and chains bearing aromatic or saturated rings were disadvantageous for the inhibition activity as shown by the lower activity of MEY-001, MEY-002, MEY-007 and MEY-008 compounds. Based on these structural requirements, we followed a funnel down synthetic and SAR approach that led to the identification of MEY-003 as the most inhibitory compound (Table 1).

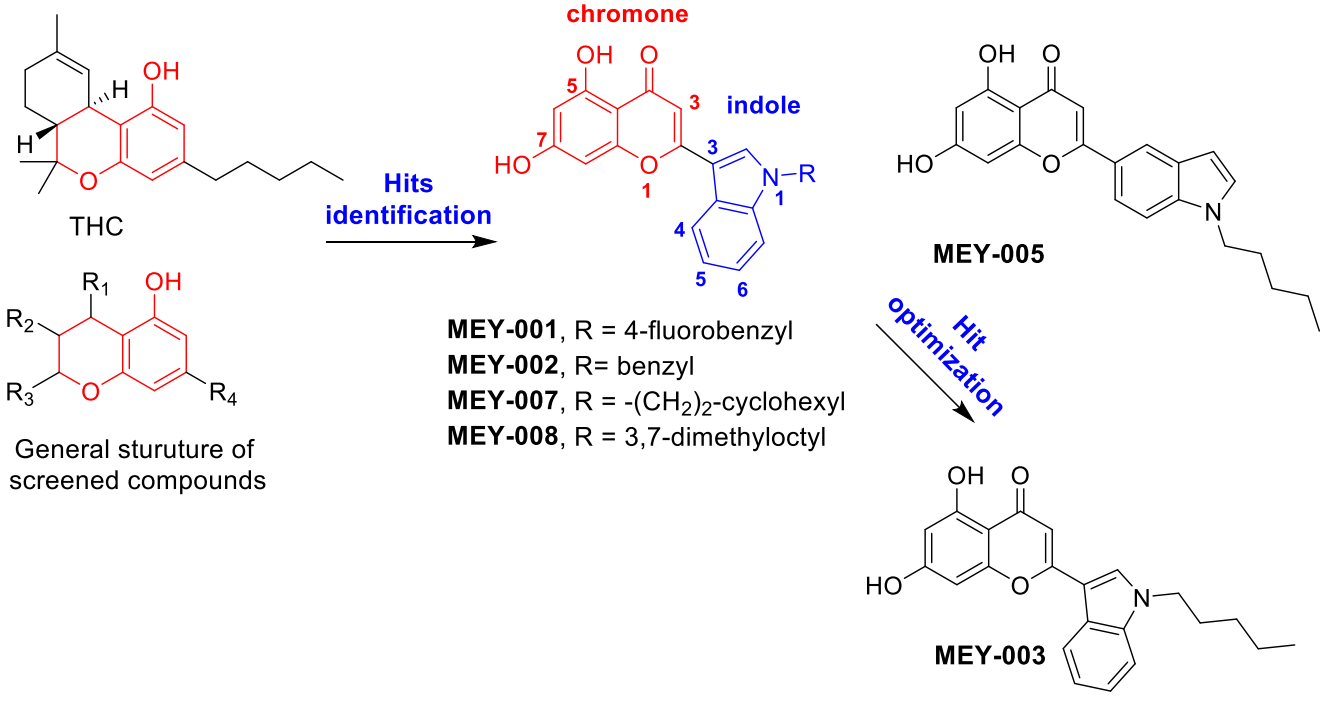

Figure 2. Discovery process of ATX inhibitors through screening and optimization of compounds sharing cannabinoid structural similarity.

Table 1. Inhibition activity of lead hits on hATX-β and hATX-ɣ.

Compound	IC_{50} hATX-β (μM)		IC_{50} hATX-ɣ (μM)	
	LPC18:1	LPC16:0	LPC18:1	LPC16:0
MEY-001	1.40 (0.9-1.8)	1.20 (0.31-1.970)	3.8(2.2-9.3)	2.4 (1.9-2.3)
MEY-002	0.82 (0.7-0.96)	0.88 (0.6-1.08)	1.25 (0.99-1.65)	0.81 (0.61-1)
MEY-003	0.46 (0.35-0.61)	0.384 (0.36-0.4)	1.099 (0.925-1.317)	0.38 (0.3-4.6)
MEY-005	> 5	> 5	> 5	> 5
MEY-007	< 20%*	< 20%*	-	-
MEY-008	NA**	NA**	-	-

* at 1 micromolar concentration; ** Not Active. Value shows 95% CI (profile likelihood)

Hits shown above (Figure 2) can be synthesized in three steps according to the same synthetic sequence as exemplified by the synthesis of MEY-003 shown in scheme 1. MEY-003 was synthesized starting from the commercially available 2,4-dimethoxy-6-hydroxyacetophenone (**1**) and *N*-pentylindol-3-carboxaldehyde (**2**). The latter can be very easily prepared by the N-alkylation of indol-3-carboxaldehyde. Starting materials (**1**) and (**2**) were subjected to a condensation reaction in the presence of potassium hydroxide in methanol to yield diarylpropenone (**3**) with 65% yield. The latter was submitted to an oxidative-cyclization reaction with iodine at 150 °C with DMSO as the solvent to provide chromone derivative (**4**) with 75% yield. Finally, compound (**4**) was subjected to boron tribromide-mediated demethylation to provide the desired compound, MEY-003, with 40% yield. The purity and authenticity of MEY-003 and its analogs shown in Figure 2 were attested by NMR (^{1}H and ^{13}C), MS (ESI+) and LCMS.

Scheme 1. Synthesis of MEY-003.

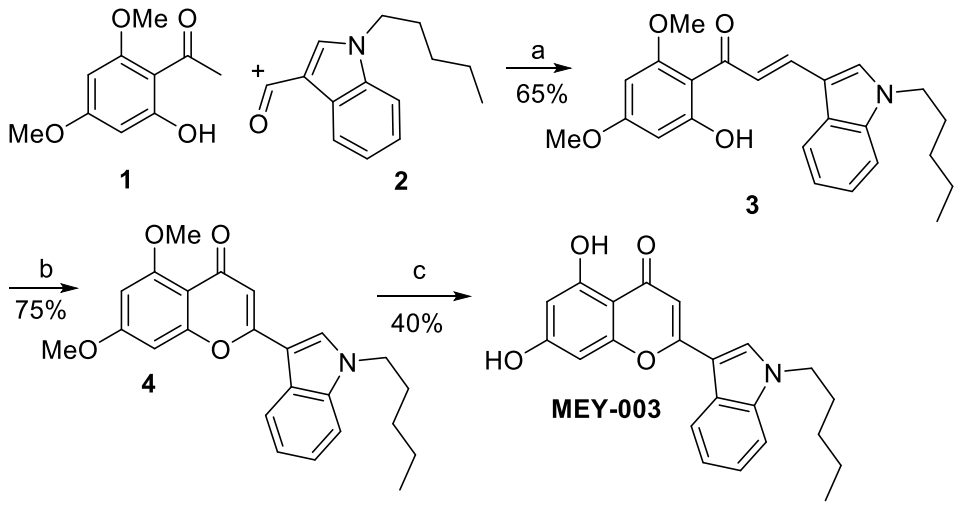

(a) KOH, MeOH, reflux, (b) I_2, DMSO, 150 °C, (c) BBr_3, CH_2Cl_2, room temperature.

As outlined above, emphasis has been focused on MEY-003 since it produced the highest inhibition level (Figure 3a, b, c, d). EC50 measurements are described in the supplemental experimental section and were adapted from our previous work using the choline-release assay.[24] The apparent EC50 with human ATX-β and LPC18:1 was 0.46 μM with an inhibition slope of 68% (Figure 3a). The apparent EC50 with human ATX-β and LPC16:0 was 0.38 μM with an inhibition slope of 83% (Figure 3c). In order to demonstrate the potency with the cerebral isoform of ATX, the apparent EC50 measurements were repeated using human ATX-ɣ under similar assay conditions. Interestingly, the apparent EC50 was slightly higher with LPC18:1, at 1.1 μM (Figure 3b), but similar to that previously obtained for hATX-β and LPC16:0, with an apparent EC50 of 0.38 μM, showing the ability of this compound to inhibit both ATX isoforms at different levels. Additionally, the span of inhibition ranged from 66% to 72% for LPC18:1 and LPC16:0, respectively.

MEY-003 acts as a non-competitive ATX inhibitor. In order to better understand the mode of action of MEY-003, an inhibition assay was run in similar assay conditions using hATX-β and LPC18:1 (Figure 3e). It shows that MEY-003 behaves as a non-competitive inhibitor (apparent Ki was 432 nM), which is in agreement with structural data (shown later). The non-competitive inhibition for MEY-003 reported

here with an Alpha value >1 can also be considered as a special case of mixed inhibition with preferential binding to the free enzyme[27].

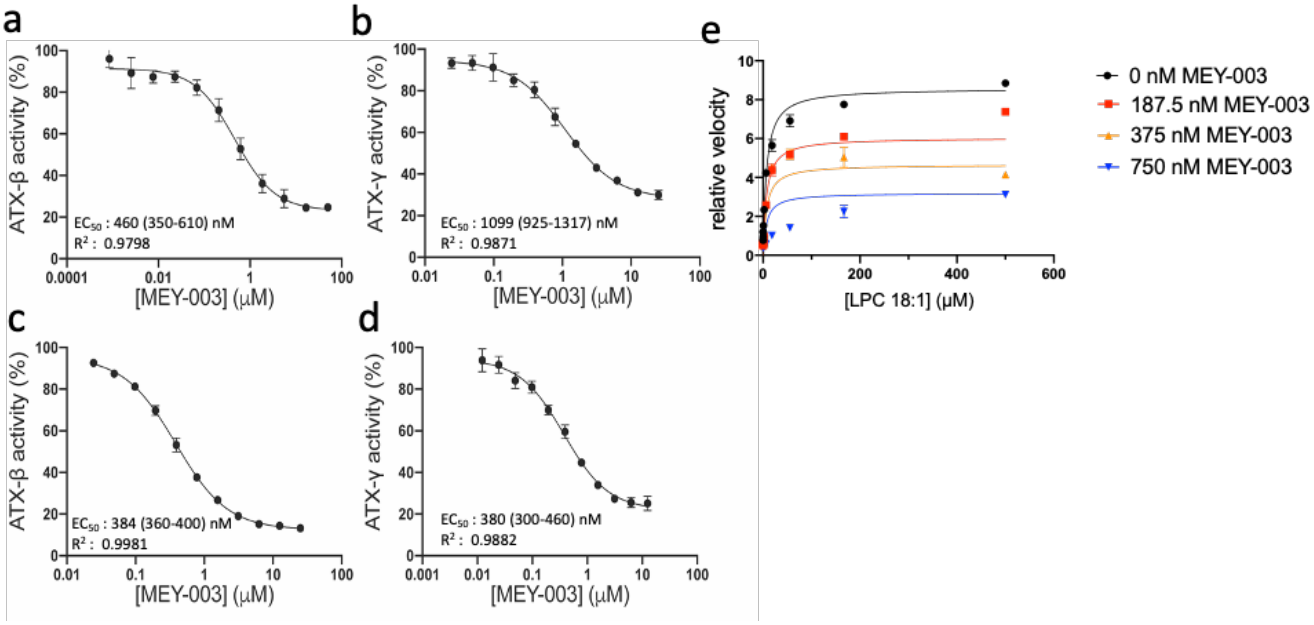

Figure 3. Inhibition of autotaxin (ATX) by MEY-003. Dose-response analysis of (a) hATX-β and (b) hATX-ɣ with LPC18:1 and MEY-003, (c) hATX-β and (d) hATX-ɣ with LPC16:0 and MEY-003. (e) The mode of inhibition of MEY-003 with hATX-β and LPC18:1 indicates a non-competitive inhibitory activity. All error bars represent the S.E.M. (n=3). EC50 values are computed with a 95% CI (profile likelihood).

MEY-003 binds in the hydrophobic pocket of ATX-ɣ. Human ATX-ɣ has been co-crystallized with MEY-003 and LPA (Table S3, Figure 4 and S1). A recombinant N54A/N411A hATX-ɣ mutant was used for crystallization as previously reported for other isoforms.[24,28] Interestingly, the enzyme crystallized in the same conditions as rat ATX-β (Supplemental experimental section), with two molecules in the asymmetric unit. The ATX-MEY-003 complex structure allowed the identification of important protein-ligand interactions in the ATX hydrophobic binding pocket using the PLIP (Protein-Ligand Interaction Profiler) server (Figure 4c and S2). Most of the interactions are hydrophobic, similar to those observed with THC and rATX-β. However, we observed two hydrogen bonds between the main chain carbonyl of W276 and

a MEY-003 hydroxy, as well as π stacking interactions between MEY-003 and residues F275 and Y307. The additional π stacking and hydrogen bonds most likely explain the difference in binding between MEY-003 and THC in the ATX hydrophobic pocket. Indeed, EC50 comparisons showed that the apparent EC50 of THC is 1.026 μM and that of MEY-003 with hATX- β and LPC18:1 is 0.46 μM. A further superposition of hATX-ɣ-MEY-003 and hATX-ɣ-LPA18:1 was carried out (Figure 4d), showing that the LPA lipophilic tail is bounded in a similar position to MEY-003 in hATX-ɣ. Additionally, a superposition with the rATX-β-THC structure from previous work shows that MEY-003 binds in a similar position, but with a slightly different conformation, to THC (Figure 4e). Interestingly, other ATX inhibitors do not seem to share a similar binding interface. For example, PAT-078, which retains an indole in its structure, does not adopt a similar conformation, at least, for the indolic part of the inhibitor (Figure 5c) (PDB: 4ZG6)[27].

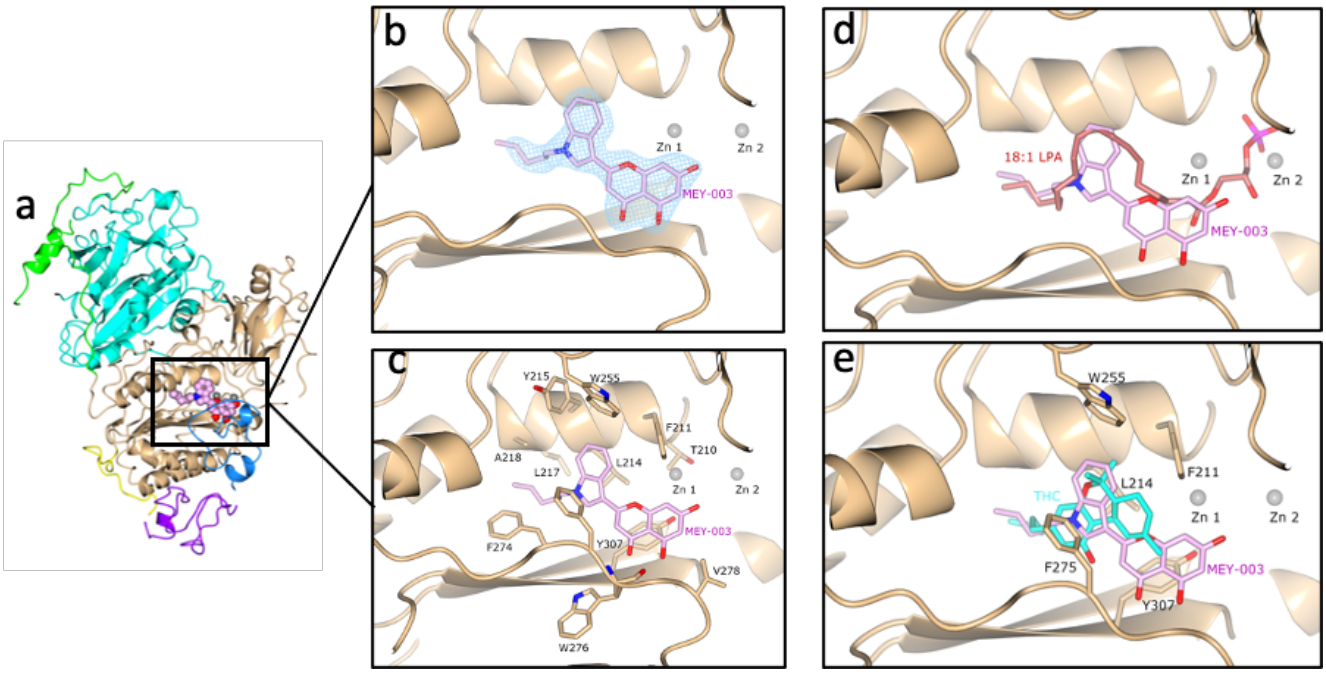

Figure 4. MEY-003 binding to hATX-ɣ hydrophobic pocket. (a) hATX-ɣ overall structure bound with MEY-003 (PDB: 8C3O). Domains are colored according to Figure 1. (b) MEY-003 $2F_O$-F_C density at 1 sigma after refinement (PDB: 8C3O). (c) MEY-003 binding interface with hATX-ɣ (PDB: 83CO). (d) Superposition of hATX-ɣ-MEY-003 and hATX-ɣ-LPA (PDB: 8C3O and 8C3P). (e) Superposition of hATX-ɣ-MEY-003 and rATX-THC with main interactions displayed (PDB: 8C3O and 7P4J).

To obtain a higher structural resolution, rATX-β was co-crystallized with both MEY-003 and MEY-002 (Table S3 and Figure 5). Superpositions of both structures showed that the indole can adopt a slightly different conformation in the hydrophobic pocket, relying on the ability of L213 to adopt two different conformations (Figure 5 d,e,f). In the MEY-003 bound structure, L213 makes a side-on interaction with the indole while adopting a face-to-face conformation with MEY-002. The MEY-002 bound structure also revealed an important water bridge in the binding interface, linking the ligand with important residues, T209 and D171, to indirectly interact with the active site Zn ions (Figure 5d). We can expect this water bridge to be relevant for MEY-003 as well, but this is probably only visible in the MEY-002-rATX-β co-structure due to the higher resolution obtained (1.9 vs 2.5 Å) (PDB: 8C4W). This might explain the non-competitive inhibition of hATX-ɣ of MEY-003 (Figure 3e). Therefore, MEY-003 could be classified as a type 2 inhibitor since it binds in the hydrophobic pocket. However, it does not completely overlap with corresponding type 2 inhibitors like PAT-078 (Figure 5c) (PDB: 4ZG6). Partial overlap with type 1 inhibitors such as HA-155 (Figure 5c) (PDB: 2XRG) shows that chromone-indol hybrid inhibitors can be classified as type 2-like inhibitors, with indirect interactions with the active site through a water bridge.

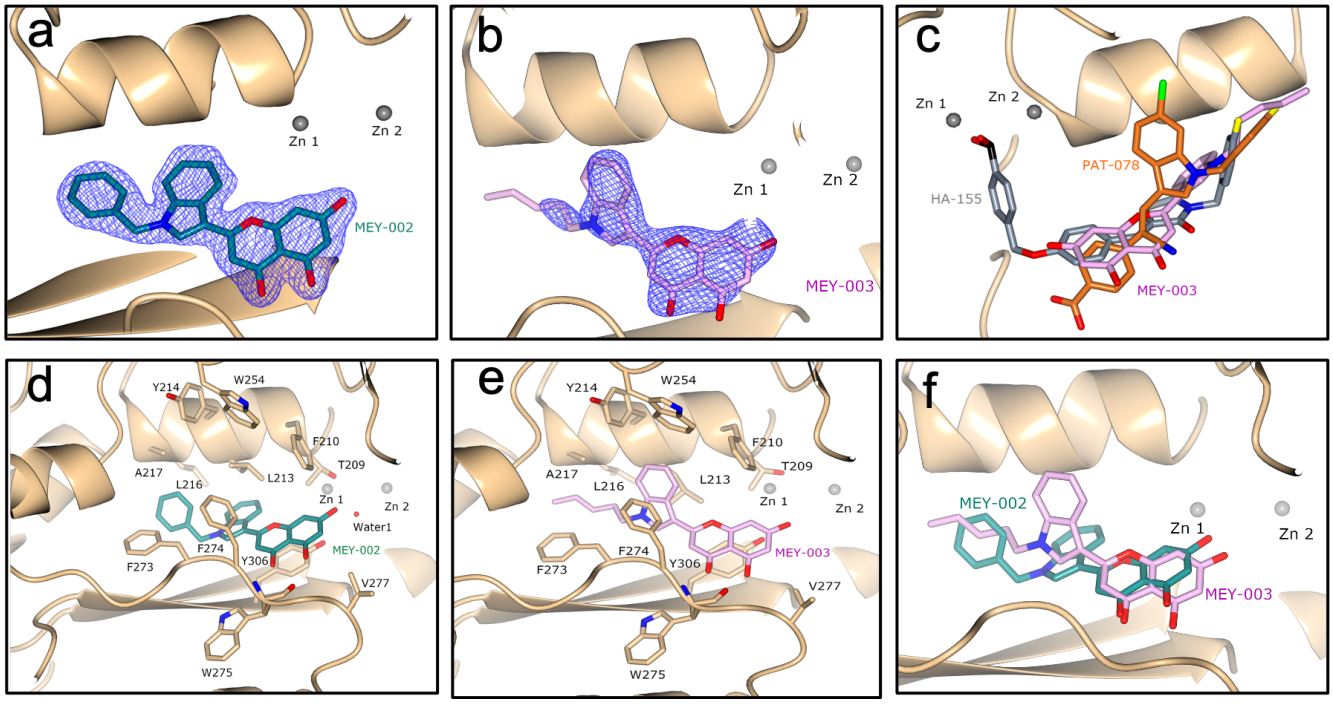

Figure 5. MEY-002 and MEY-003 binding to the rATX-β hydrophobic pocket. (a) MEY-002 $2F_O$-F_C density at 1 sigma after refinement (PDB: 8C4W). (b) MEY-003 $2F_O$-F_C density at 1 sigma after refinement (PDB: 8C7R). (c) Superposition of inhibitors HA-155, PAT-078 and MEY-003 (PDB: 2XRG, 4ZG6 and 8C7R). (d) MEY-002 binding interface with rATX-β (PDB:8C4W). (e) MEY-003 binding interface-with rATX-β (PDB: 8C7R). (f) Superposition of rATX-β-MEY-002 and rATX-β-MEY-003 (PDB: 8C4W and 8C7R).

MEY-003 reduces hLPAR1 internalization and is not cytotoxic to HeLa cells. ATX regulates various physiological and pathological processes in cells. One of the key roles of ATX is to produce LPA, a major lipid cell signaling component. Previous studies showed that the ATX-LPA axis is highly regulated and dependent on ATX activity in order to trigger LPA receptor internalization.[8] It has been recently demonstrated that ATX is responsible for LPA presentation towards receptors by acting as a chaperone. [20] In this study, we confirmed that MEY-003 is able to reduce LPA1 receptor internalization in HeLa cells after treatment with LPC and hATX-β. LPA1 internalization was reduced by approximatively 47% (Figure 6a), showing that MEY-003 significantly blocks LPA signaling through ATX inhibition. Moreover, further *in*

vitro assays showed that MEY-003 is non-cytotoxic after prolonged treatment (up to 8 hours) at 100 µM. The same assay performed on MEY-002 also showed no cytotoxicity effects (Figure 6b).

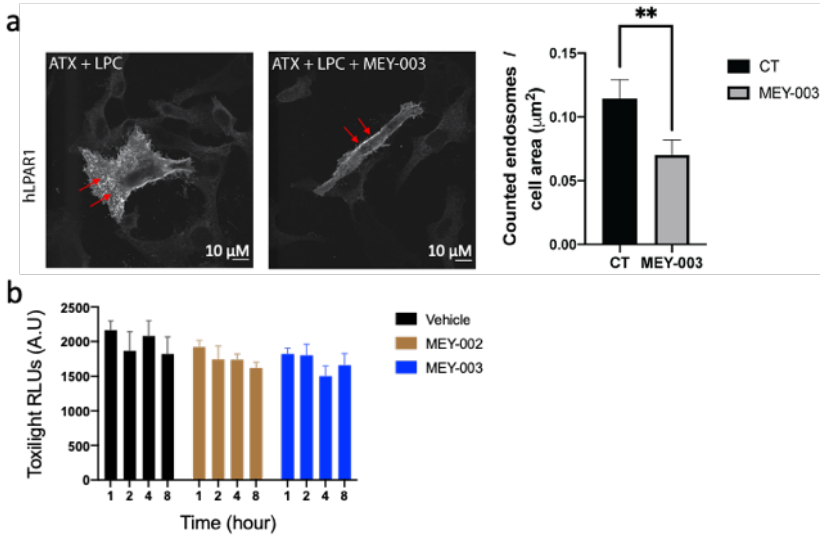

Figure 6. MEY-003 reduces LPA1 receptor internalization and is not cytotoxic to HeLa cells. (a) Cells were treated with hATX-β and LPC with or without MEY-003 addition. After treatment, cells were fixed and stained using an anti-HA tag antibody. 17 and 15 images were acquired in biological triplicate for hATX-β + LPC + MEY-003 and hATX-β + LPC, respectively, using a LEICA microscope at 63X magnification. Red arrows are pointing at LPA1 receptor hypersignal. Receptor internalization was quantified with Fiji with a paired t-test p-value = 0.0078. (b) Cells were incubated with 100 µM of MEY-003 or MEY-002 for 1 to 8 hours. Cytotoxicity detection was performed using Toxilight assay. All error bars represent S.E.M. (n=3) in biological triplicate.

■ DISCUSSION

The plant *Cannabis sativa* (Marijuana) has been used in medicine for a long time and still attracts interest due to the biological activity of its metabolites, known as cannabinoids (a group of C21 terpenophenolic compounds). The most abundant among them is Δ9-tetrahydrocannabinol (THC). Marijuana-derived drugs, and especially those derived from THC, have been developed but their therapeutic/psychotropic balance was frequently criticized. In this study, we have used the general chemical structure of THC that

showed an inhibitory activity against ATX as a basis to screen chemical libraries sharing some structural similarities with THC, but derived from different secondary metabolites. Hence, following the screening of a chemical library of compounds bearing the benzopyranone moiety (Supplemental section II) and the optimization of the obtained selected hits (Figure 2 and Table 1), we identified the compound MEY-003, which is derived from a hybrid system bearing both chromone and indole scaffolds as a potent inhibitor of ATX (Figure 3).

Here, we also describe the structure of hATX-ɣ in complex with its natural end-product LPA18:1 and MEY-003 at a resolution of 2.4 and 2.3 Å, respectively (Figure 4). Our results highlight that hATX-ɣ shares a very similar structural organization with hATX-β, as deduced from superposition with the PDB: 4ZG7,[27] resulting in an RMSD of 0.56 Å for 775 aligned Cα atoms. The deglycosylated mutant used for crystallization did not lead to a significant activity difference when compared to wild-type hATX-ɣ (Figure S3). One major difference between the brain-specific hATX-ɣ and hATX-β is the presence of a 25 aa insertion at position 593 (EAETRKFRGSRNENKENINGNFEPRK), leading to a flexible loop at the surface of hATX-ɣ. The function of this modification is unknown and specific to the brain isoform. Up to now, there is no evidence that proteolytic cleavage of this loop is related to neurological, psychiatric and neoplasic diseases.[16,17,29] In this study, we also observed that hATX-ɣ can be cleaved (Figure S4), resulting in a fragment of ~34 kDa that corresponds to a C-terminal region cleavage at this insertion. Further experiments would be needed to understand which enzyme is responsible for cleaving hATX-ɣ and if this is biologically relevant.

Chromones and indoles are two prominent scaffolds largely investigated for their therapeutic potential in the management of major chronic diseases, including neurodegenerative diseases, cancer, diabetes, infection and inflammation.[25,30] The physicochemical properties of MEY-003 are promising, with a calculated logP of 3.7, a MW of 363.41 Da, as well as 2 and 5 hydrogen bond donors and acceptors, respectively (Table S2). MEY-003 respects the Lipinski's rule for oral bioavailability and fits most of the properties described by Pajouhesh *et al*. for successful central nervous system drugs, with a calculated PSA of 70 Å and previously described properties [31]. Concerning the metabolic liability of the chromone, a good *in vivo*

stability of this scaffold has previously been reported [32]. In addition, Cromolyn, a drug used for allergies and composed of a chromone scaffold has also been shown to have good metabolic stability, with most of the compound excreted without modifications [33]. In latter contexts, many clinically approved drugs contain one of these two entities.[25] Therefore, the combination of a chromone and an indole, two druggable scaffolds, in the same entity may offer diverse advantages for the development of MEY-003 as a drug candidate that targets ATX-related diseases.

■ CONCLUSION

We recently reported that THC is a potent ATX inhibitor.[24] Due to its psychotropic effect, legislation, and non-acceptance by society, this marijuana-derived compound is unlikely to be used in clinical settings for the management of ATX-related disorders. Therefore, we used THC as a basis to explore diverse molecules with partial chemical and structural similarity, particularly those sharing a benzopyrane moiety such as naturally occurring chromones and flavones. The process of screening, hit identification and hit optimization allowed us to identify MEY-003 as a potent and safe inhibitor of ATX. The inhibition profile of MEY-003 was rationalized through advanced structural biology drug discovery studies. MEY-003 has a unique structure compared to previously published ATX inhibitors that could potentially lead to the development of new drugs targeting the ATX-LPA axis with fewer side effects.

■ ASSOCIATED CONTENT

SUPPORTING INFORMATION

The Supporting Information is available free of charge at https://pubs.acs.org

Synthesis methods and characterization of MEY-003 analogs. Spectral data, inhibitor summary, biochemical reagents and crystallographic data.

PDB accession codes for the presented structures: atomic coordinates and experimental data will be released upon article publication (see table S3 for PDB codes).

■ AUTHOR INFORMATION

Corresponding Authors

Andrew A. McCarthy - *European Molecular Biology Laboratory, EMBL Grenoble, 71 avenue des Martyrs, 38000 Grenoble, France*

Ahcène Boumendjel – *Univ. Grenoble Alpes, INSERM, LRB, 38000 Grenoble, France*

Authors

Mathias Christophe Eymery - *European Molecular Biology Laboratory, EMBL Grenoble, 71 avenue des Martyrs, 38000 Grenoble, France*

Kim-Anh Nguyen - *Univ. Grenoble Alpes, INSERM, LRB, 38000 Grenoble, France*

Shibom Basu - *European Molecular Biology Laboratory, EMBL Grenoble, 71 avenue des Martyrs, 38000 Grenoble, France*

Jens Hausmann - *European Molecular Biology Laboratory, EMBL Grenoble, 71 avenue des Martyrs, 38000 Grenoble, France. Current address: School of Medicine and Health Sciences, Carl von Ossietzky University of Oldenburg, Oldenburg, Germany.*

Viet-Khoa Tran-Nguyen - *Centre de Recherche en Cancérologie de Marseille (CRCM), Inserm, U1068, Marseille, F-13009, France*

Hans Peter Seidel - *European Molecular Biology Laboratory, EMBL Grenoble, 71 avenue des Martyrs, 38000 Grenoble, France*

Lola Gutierrez - *European Molecular Biology Laboratory, EMBL Grenoble, 71 avenue des Martyrs, 38000 Grenoble, France*

Author Contributions

M.C.E. Development of methodology, acquisition of data, analysis and interpretation of results. K.A.N. Organic synthesis of hits and MEY-003. S.B., J.H., H.P.S and L.G. Structural biology studies and interpretation of results. V.K.T.N. Molecular modelling and docking studies. A.B. and A.A.M. Conception, design and study supervision. The manuscript was written through the contributions of all authors. All authors read and approved the final version of the manuscript.

Notes

Findings regarding the potential applications of MEY-003 and analogs are the subject of E.U. patent application EP22215403.1, filed on December 21, 2022, owned by European Molecular Biology Laboratory, and Université Grenoble Alpes, and lists M.C.E., A.B., and A.A.M as inventors.

■ ACKNOWLEDGMENT

We are thankful for the kind gift of ATX-expressing cell lines from the Perrakis laboratory at NKI in Amsterdam. We thank the beamline staff from the EMBL-ESRF Joint Structural Biology Group for beamtime at the European Synchrotron Radiation Facility (ESRF), Grenoble, France. The authors also wish to express their gratitude to the Eukaryotic Expression Facility in Grenoble for infrastructure access, especially Alice Aubert and Martin Pelosse for excellent technical support and fruitful discussions. MC Eymery has been funded by the EMBL International PhD program. AA McCarthy has been funded by EMBL. J Hausmann was supported by a fellowship from the EMBL Interdisciplinary Postdoc (EI3POD) program under Marie Skłodowska-Curie Actions COFUND (grant number: 664726).

■ ABBREVIATIONS

ATX, autotaxin; FCS, fetal calf serum; HRP, horseradish peroxidase; LPA, lysophosphatidic acid; LPC, lysophosphatidyl choline; MTBE, methyl tert-butyl ether; NUC, nuclease; PDB, protein data bank; PDE, phosphodiesterase; SEM, standard error of the mean; SMB, somatomedin β-like.

■ REFERENCES

(1) Ninou, I.; Magkrioti, C.; Aidinis, V. Autotaxin in Pathophysiology and Pulmonary Fibrosis. *Front. Med.* **2018**, *5*, 180. https://doi.org/10.3389/fmed.2018.00180.

(2) Castagna, D.; Budd, D. C.; Macdonald, S. J. F.; Jamieson, C.; Watson, A. J. B. Development of Autotaxin Inhibitors: An Overview of the Patent and Primary Literature: Miniperspective. *Journal of Medicinal Chemistry* **2016**, *59* (12), 5604–5621. https://doi.org/10.1021/acs.jmedchem.5b01599.

(3) Ninou, I.; Magkrioti, C.; Aidinis, V. Autotaxin in Pathophysiology and Pulmonary Fibrosis. *Frontiers in Medicine* **2018**, *5*. https://doi.org/10.3389/fmed.2018.00180.

(4) Giganti, A.; Rodriguez, M.; Fould, B.; Moulharat, N.; Cogé, F.; Chomarat, P.; Galizzi, J.-P.; Valet, P.; Saulnier-Blache, J.-S.; Boutin, J. A.; Ferry, G. Murine and Human Autotaxin α, β, and γ Isoforms. *Journal of Biological Chemistry* **2008**, *283* (12), 7776–7789. https://doi.org/10.1074/jbc.M708705200.

(5) Hashimoto, T.; Okudaira, S.; Igarashi, K.; Hama, K.; Yatomi, Y.; Aoki, J. Identification and Biochemical Characterization of a Novel Autotaxin Isoform, ATX , with a Four-Amino Acid Deletion. *Journal of Biochemistry* **2012**, *151* (1), 89–97. https://doi.org/10.1093/jb/mvr126.

(6) *RCSB Protein Data Bank - RCSB PDB*. http://www.rcsb.org/pdb/home/home.do (accessed 2017-12-09).

(7) Moolenaar, W. H.; Perrakis, A. Insights into Autotaxin: How to Produce and Present a Lipid Mediator. *Nat Rev Mol Cell Biol* **2011**, *12* (10), 674–679. https://doi.org/10.1038/nrm3188.

(8) Gotoh, M.; Fujiwara, Y.; Yue, J.; Liu, J.; Lee, S.; Fells, J.; Uchiyama, A.; Murakami-Murofushi, K.; Kennel, S.; Wall, J.; Patil, R.; Gupte, R.; Balazs, L.; Miller, D. D.; Tigyi, G. J. Controlling Cancer through the Autotaxin–Lysophosphatidic Acid Receptor Axis. *Biochemical Society Transactions* **2012**, *40* (1), 31–36. https://doi.org/10.1042/BST20110608.

(9) Lee, D.; Suh, D.-S.; Lee, S. C.; Tigyi, G. J.; Kim, J. H. Role of Autotaxin in Cancer Stem Cells. *Cancer and Metastasis Reviews* **2018**, *37* (2–3), 509–518. https://doi.org/10.1007/s10555-018-9745-x.

(10) Umezu-Goto, M.; Kishi, Y.; Taira, A.; Hama, K.; Dohmae, N.; Takio, K.; Yamori, T.; Mills, G. B.; Inoue, K.; Aoki, J.; Arai, H. Autotaxin Has Lysophospholipase D Activity Leading to Tumor Cell Growth and Motility by Lysophosphatidic Acid Production. *The Journal of Cell Biology* **2002**, *158* (2), 227–233. https://doi.org/10.1083/jcb.200204026.

(11) Valdés-Rives, S. A.; González-Arenas, A. Autotaxin-Lysophosphatidic Acid: From Inflammation to Cancer Development. *Mediators of Inflammation* **2017**, *2017*, 1–15. https://doi.org/10.1155/2017/9173090.

(12) Willier, S.; Butt, E.; Grunewald, T. G. P. Lysophosphatidic Acid (LPA) Signalling in Cell Migration and Cancer Invasion: A Focussed Review and Analysis of LPA Receptor Gene Expression on the Basis of More than 1700 Cancer Microarrays: Role of LPA in Cell Migration and Cancer Metastasis. *Biol. Cell* **2013**, *105* (8), 317–333. https://doi.org/10.1111/boc.201300011.

(13) Achón Buil, B.; Rust, R. Preserving Stroke Penumbra by Targeting Lipid Signalling. *Journal of Cerebral Blood Flow & Metabolism* **2023**, *43* (1), 167–169. https://doi.org/10.1177/0271678X221121853.
(14) Alioli, C.; Demesmay, L.; Peyruchaud, O.; Machuca-Gayet, I. Autotaxin/Lysophosphatidic Acid Axis: From Bone Biology to Bone Disorders. *IJMS* **2022**, *23* (7), 3427. https://doi.org/10.3390/ijms23073427.
(15) Dohi, T.; Miyauchi, K.; Ohkawa, R.; Nakamura, K.; Kishimoto, T.; Miyazaki, T.; Nishino, A.; Nakajima, N.; Yaginuma, K.; Tamura, H.; Kojima, T.; Yokoyama, K.; Kurata, T.; Shimada, K.; Yatomi, Y.; Daida, H. Increased Circulating Plasma Lysophosphatidic Acid in Patients with Acute Coronary Syndrome. *Clinica Chimica Acta* **2012**, *413* (1), 207–212. https://doi.org/10.1016/j.cca.2011.09.027.
(16) Herr, D. R.; Chew, W. S.; Satish, R. L.; Ong, W.-Y. Pleotropic Roles of Autotaxin in the Nervous System Present Opportunities for the Development of Novel Therapeutics for Neurological Diseases. *Molecular Neurobiology* **2020**, *57* (1), 372–392. https://doi.org/10.1007/s12035-019-01719-1.
(17) for the Alzheimer's Disease Neuroimaging Initiative; McLimans, K. E.; Willette, A. A. Autotaxin Is Related to Metabolic Dysfunction and Predicts Alzheimer's Disease Outcomes. *JAD* **2017**, *56* (1), 403–413. https://doi.org/10.3233/JAD-160891.
(18) Tigyi, G. Aiming Drug Discovery at Lysophosphatidic Acid Targets: Novel LPA Targets. *British Journal of Pharmacology* **2010**, *161* (2), 241–270. https://doi.org/10.1111/j.1476-5381.2010.00815.x.
(19) Taniguchi, R.; Inoue, A.; Sayama, M.; Uwamizu, A.; Yamashita, K.; Hirata, K.; Yoshida, M.; Tanaka, Y.; Kato, H. E.; Nakada-Nakura, Y.; Otani, Y.; Nishizawa, T.; Doi, T.; Ohwada, T.; Ishitani, R.; Aoki, J.; Nureki, O. Structural Insights into Ligand Recognition by the Lysophosphatidic Acid Receptor LPA6. *Nature* **2017**, *548* (7667), 356–360. https://doi.org/10.1038/nature23448.
(20) Salgado-Polo, F.; Borza, R.; Matsoukas, M.-T.; Marsais, F.; Jagerschmidt, C.; Waeckel, L.; Moolenaar, W. H.; Ford, P.; Heckmann, B.; Perrakis, A. Autotaxin Facilitates Selective LPA Receptor Signaling. *Cell Chemical Biology* **2023**, *30* (1), 69-84.e14. https://doi.org/10.1016/j.chembiol.2022.12.006.
(21) Albers, H. M. H. G.; Hendrickx, L. J. D.; van Tol, R. J. P.; Hausmann, J.; Perrakis, A.; Ovaa, H. Structure-Based Design of Novel Boronic Acid-Based Inhibitors of Autotaxin. *Journal of Medicinal Chemistry* **2011**, *54* (13), 4619–4626. https://doi.org/10.1021/jm200310q.
(22) Keune, W.-J.; Potjewyd, F.; Heidebrecht, T.; Salgado-Polo, F.; Macdonald, S. J. F.; Chelvarajan, L.; Abdel Latif, A.; Soman, S.; Morris, A. J.; Watson, A. J. B.; Jamieson, C.; Perrakis, A. Rational Design of Autotaxin Inhibitors by Structural Evolution of Endogenous Modulators. *Journal of Medicinal Chemistry* **2017**, *60* (5), 2006–2017. https://doi.org/10.1021/acs.jmedchem.6b01743.
(23) Miller, L. M.; Keune, W.-J.; Castagna, D.; Young, L. C.; Duffy, E. L.; Potjewyd, F.; Salgado-Polo, F.; Engel García, P.; Semaan, D.; Pritchard, J. M.; Perrakis, A.; Macdonald, S. J. F.; Jamieson, C.; Watson, A. J. B. Structure–Activity Relationships of Small Molecule Autotaxin Inhibitors with a Discrete Binding Mode. *Journal of Medicinal Chemistry* **2017**, *60* (2), 722–748. https://doi.org/10.1021/acs.jmedchem.6b01597.
(24) Eymery, M. C.; McCarthy, A. A.; Hausmann, J. Linking Medicinal Cannabis to Autotaxin–Lysophosphatidic Acid Signaling. *Life Science Alliance* **2023**, *6* (2), e202201595. https://doi.org/10.26508/lsa.202201595.
(25) Reis, J.; Gaspar, A.; Milhazes, N.; Borges, F. Chromone as a Privileged Scaffold in Drug Discovery: Recent Advances: Miniperspective. *Journal of Medicinal Chemistry* **2017**, *60* (19), 7941–7957. https://doi.org/10.1021/acs.jmedchem.6b01720.
(26) Gaspar, A.; Matos, M. J.; Garrido, J.; Uriarte, E.; Borges, F. Chromone: A Valid Scaffold in Medicinal Chemistry. *Chemical Reviews* **2014**, *114* (9), 4960–4992. https://doi.org/10.1021/cr400265z.

(27) Stein, A. J.; Bain, G.; Prodanovich, P.; Santini, A. M.; Darlington, J.; Stelzer, N. M. P.; Sidhu, R. S.; Schaub, J.; Goulet, L.; Lonergan, D.; Calderon, I.; Evans, J. F.; Hutchinson, J. H. Structural Basis for Inhibition of Human Autotaxin by Four Potent Compounds with Distinct Modes of Binding. *Molecular Pharmacology* **2015**, *88* (6), 982–992. https://doi.org/10.1124/mol.115.100404.
(28) Hausmann, J.; Kamtekar, S.; Christodoulou, E.; Day, J. E.; Wu, T.; Fulkerson, Z.; Albers, H. M. H. G.; van Meeteren, L. A.; Houben, A. J. S.; van Zeijl, L.; Jansen, S.; Andries, M.; Hall, T.; Pegg, L. E.; Benson, T. E.; Kasiem, M.; Harlos, K.; Kooi, C. W. V.; Smyth, S. S.; Ovaa, H.; Bollen, M.; Morris, A. J.; Moolenaar, W. H.; Perrakis, A. Structural Basis of Substrate Discrimination and Integrin Binding by Autotaxin. *Nature Structural & Molecular Biology* **2011**, *18* (2), 198–204. https://doi.org/10.1038/nsmb.1980.
(29) Herr, D. R.; Ong, J. H.-J.; Ong, W.-Y. Potential Therapeutic Applications for Inhibitors of Autotaxin, a Bioactive Lipid-Producing Lysophospholipase D, in Disorders Affecting the Nervous System. *ACS Chemical Neuroscience* **2018**, *9* (3), 398–400. https://doi.org/10.1021/acschemneuro.8b00057.
(30) Eymery, M.; Tran-Nguyen, V.-K.; Boumendjel, A. Diversity-Oriented Synthesis: Amino Acetophenones as Building Blocks for the Synthesis of Natural Product Analogs. *Pharmaceuticals* **2021**, *14* (11), 1127. https://doi.org/10.3390/ph14111127.
(31) Pajouhesh, H.; Lenz, G. R. Medicinal Chemical Properties of Successful Central Nervous System Drugs. *Neurotherapeutics* **2005**, *2* (4), 541–553. https://doi.org/10.1602/neurorx.2.4.541.
(32) Csepanyi, E.; Szabados-Furjesi, P.; Kiss-Szikszai, A.; Frensemeier, L. M.; Karst, U.; Lekli, I.; Haines, D. D.; Tosaki, A.; Bak, I. Antioxidant Properties and Oxidative Transformation of Different Chromone Derivatives. *Molecules* **2017**, *22* (4), 588. https://doi.org/10.3390/molecules22040588.
(33) Ashton, M. J.; Clark, B.; Jones, K. M.; Moss, G. F.; Neale, M. G.; Ritchie, J. T. The Absorption, Metabolism and Excretion of Disodium Cromoglycate in Nine Animal Species. *Toxicology and Applied Pharmacology* **1973**, *26* (3), 319–328. https://doi.org/10.1016/0041-008X(73)90268-8.